eNeuro

Research Article: New Research | Sensory and Motor Systems

Heterozygous *Dcc* mutant mice have a subtle locomotor phenotype

https://doi.org/10.1523/ENEURO.0216-18.2021

Cite as: eNeuro 2022; 10.1523/ENEURO.0216-18.2021

Received: 31 May 2018
Revised: 18 December 2021
Accepted: 20 December 2021

Title: Heterozygous *Dcc* mutant mice have a subtle locomotor phenotype

Abbreviated title: Locomotor functions in *Dcc* heterozygous mice

Authors: Louise Thiry[1,*], Chloé Lemaire[1,*], Ali Rastqar[1,*], Maxime Lemieux[1,*], Jimmy Peng[2,3,*], Julien Ferent[2,3], Marie Roussel[1], Eric Beaumont[4], James P. Fawcett[5,6], Robert M. Brownstone[7], Frédéric Charron[2,3,8,#], Frédéric Bretzner[1,9,#]

[1] Centre de Recherche du CHU de Québec-Université Laval, CHUL – Neurosciences P09800, 2705 boul. Laurier, Quebec City, Quebec Canada, G1V 4G2

[2] Institut de Recherches Cliniques de Montréal (IRCM), Montréal, Quebec, Canada

[3] Department of Biology, McGill University, Montréal, Quebec, Canada

[4] Department of Biomedical Sciences, Quillen College of Medicine, East Tennessee State University, Johnson City, Tennessee, 37604.

[5] Department of Pharmacology, Dalhousie University, Halifax, Nova Scotia Canada, B3H 4R2

[6] Department of Surgery, Dalhousie University, Halifax, Nova Scotia, Canada, B3H 4R2

[7] UCL Queen Square Institute of Neurology, University College London, London, UK WC1N 3BG

[8] Department of Medicine, University of Montreal, Montréal, Quebec, Canada

[9] Department of Psychiatry and Neurosciences, Université Laval, Quebec City, Quebec Canada, G1V 4G2

*Equal contribution

Co-senior authors

Author Contributions: RMB, JPF, FC and FB designed research; JP and EB performed in vivo tracing; LT, CL, AR, ML, MR, and FB performed electrophysiological and behavioral experiments and analyzed data; JF analyzed Dcc levels in spinal cords; LT, CL, ML, JP, FC, and FB wrote the paper. RMB, JPF, FC, and FB edited the paper.

Corresponding authors: Frédéric Charron and Frédéric Bretzner

E-mail: frederic.charron@ircm.qc.ca

E-mail: frederic.bretzner.1@ulaval.ca

Number of pages: 24

Number of figures, tables and multimedia: 11 Figures, 0 tables, 0 multimedia

Number of words: 208 words for the abstract, 65 for the significance statement, 814 for the introduction, 1460 for the discussion

Acknowledgments: We thank Béatrice Frenette for technical help. This work was supported by grants from the Canadian Institutes of Health Research (CIHR) (334023), the Fonds de Recherche du Québec - Santé (FRQS) (27003), and the Canada Foundation for Innovation (CFI) (33768) to FC; CIHR to JPF (MOP 341174); CIHR to RMB (79413); and the Natural Sciences and Engineering Research Council of Canada (NSERC, 2018-06218) to FB. JP was funded by a CIHR Vanier Canada Graduate scholarship. JF was funded by FRQS and CIHR fellowships. FC holds the Canada Research Chair in Developmental Neurobiology. FB is a Fonds de Recherche du Québec - Santé (FRQS) Chercheur-Boursier (284011).

Conflict of interest: The authors declare no competing financial interest.

Title: Heterozygous *Dcc* mutant mice have a subtle locomotor phenotype

Abbreviated title: Locomotor functions in *Dcc* heterozygous mice

ABSTRACT

Axon guidance receptors such as DCC contribute to the normal formation of neural circuits, and their mutations can be associated with neural defects. In humans, heterozygous mutations in *DCC* have been linked to congenital mirror movements, which are involuntary movements on one side of the body that mirror voluntary movements of the opposite side. In mice, obvious hopping phenotypes have been reported for bi-allelic *Dcc* mutations, while heterozygous mutants have not been closely examined. We hypothesized that a detailed characterization of *Dcc* heterozygous mice may reveal impaired corticospinal and spinal functions. Anterograde tracing of the $Dcc^{+/-}$ motor cortex revealed a normally projecting corticospinal tract, intracortical microstimulation evoked normal contralateral motor responses, and behavioral tests showed normal skilled forelimb coordination. Gait analyses also showed a normal locomotor pattern and rhythm in adult $Dcc^{+/-}$ mice during treadmill locomotion, except for a decreased occurrence of out-of-phase walk and an increased duty cycle of the stance phase at slow walking speed. Neonatal isolated $Dcc^{+/-}$ spinal cords had normal left-right and flexor-extensor coupling, along with normal locomotor pattern and rhythm, except for an increase in the flexor-related motoneuronal output. Although $Dcc^{+/-}$ mice do not exhibit any obvious bilateral impairments like those in humans, they exhibit subtle motor deficits during neonatal and adult locomotion.

SIGNIFICANCE STATEMENT

We show that loss of one *Dcc* allele does not affect motor cortex, corticospinal efficacy, or skilled locomotor control in adult mice, but it increases flexor-related motoneuronal output in the developing spinal cord and increases duty cycle of the stance phase during treadmill locomotion at slow walking speeds in adult mice. This finding raises the possibility of the existence of subtle locomotor changes in humans carrying monoallelic *DCC* mutations.

INTRODUCTION

Individuals carrying monoallelic *DCC* (Deleted in Colorectal Cancer) mutations exhibit congenital mirror movements, which are unintentional movements on one side of the body that are mirror reversals of intended unilateral movements on the opposite side (Schott and Syke, 1981; Srour et al., 2010). Bilateral motor responses can be evoked in response to unilateral transcranial magnetic stimulation of the motor cortex in these people (Srour et al., 2010; Welniarz et al., 2017) and, these bilateral motor responses are correlated with an abnormal bilateral projection of their corticospinal fibers at the level of the pyramidal decussation (Welniarz et al., 2017). This phenotype in *DCC* heterozygous humans is most likely a result of haplo-insufficiency, given that many of the mutations are predicted to result in mRNA degradation or truncated DCC proteins (Izzi and Charron, 2011; Peng and Charron, 2013). The receptor DCC mediates a chemoattractive signal to Netrin-1 (Keino-Masu et al., 1996; Fazeli et al., 1997; Jain et al., 2014; Srivatsa et al., 2014), thereby contributing to the normal development of a wide variety of axonal tracts, including those of spinal commissural interneurons (Rabe Bernhardt et al., 2012) and corticospinal tracts (Finger et al., 2012). Mutations in *NETRIN-1* also cause mirror movements in human (Méneret et al., 2017). Loss of floor plate Netrin-1 in mice impairs midline crossing of corticospinal and spinal axons and leads to a bilateral forelimb movement phenotype reminiscent of human mirror movements (Pourchet et al., 2021).

In contrast to $DCC^{+/-}$ humans, heterozygous $Dcc^{+/-}$ mice exhibit no overt mirror-like phenotypes. Bi-allelic *Dcc* null mutant mice die at birth, precluding the possibility of studying their motor cortex and corticospinal tract projection through adulthood (Fazeli

et al., 1997). However, mutant mice carrying the bi-allelic *kanga* mutation (*Dcc*$^{kanga/kanga}$), a spontaneous mutation that removes the P3 intracellular domain, are viable and exhibit an abnormal rabbit-like hopping gait (Finger et al., 2002). The hopping gait phenotype is different from the bilateral forelimb movement phenotype: while the former is mostly known to occur due to axon crossing defects in spinal interneurons (Peng et al., 2018; Kullander et al., 2003; Talpalar et al., 2013), the latter has been linked to crossing defects of the corticospinal tract (Pourchet et al., 2021; Serradj et al., 2014). Corticospinal tract lateralization defects produce phenotypes more akin to the mirror-movement phenotype observed in *DCC*$^{+/-}$ humans.

DCC and its ligand Netrin-1 are also important for normal development of sensory afferents to the dorsal spinal cord (Ding et al., 2005; Watanabe et al., 2006) and spinal commissural interneurons (Keino-Masu et al., 1996; Fazeli et al., 1997; Rabe et al., 2009; Rabe Bernhardt et al., 2012; Dominici et al., 2017; Varadarajan et al., 2017). Spinal cords isolated from neonatal wild-type mice produce spontaneous left-right alternating neuronal activity upon bath application of neurotransmitters, which reflect the output of the locomotor central pattern generator (Jiang et al., 1999; Thiry et al., 2016). Interestingly, neonatal *Netrin-1* mutant spinal cords exhibit a reduction in the number of commissural interneurons including V0 commissural interneurons, whereas V3 commissural interneurons are spared and presumably contribute to the synchronization of left and right locomotor activities (Rabe Bernhardt et al., 2012). However, both neonatal *Dcc*$^{-/-}$ and *Dcc*$^{kanga/kanga}$ spinal cords exhibit a robust reduction in the number of most commissural interneurons, including V0 and V3 commissural interneurons, thus leading to disorganization of the coupling between left and right

locomotor activities (Rabe Bernhardt et al., 2012). More recently, it has been shown that a selective *Dcc* mutation in spinal interneurons (*HoxB8^{cre}; Dcc$^{flox/-}$* and *HoxB8^{cre}; Dcc$^{flox/flox}$*) exhibits a robust hopping phenotype in adult mice (Peng et al., 2018), indicating that local spinal cord defects following loss of *Dcc* cause a hopping gait. Given the strong phenotype reported in various neonatal and adult biallelic *Dcc* mutant spinal cords, we hypothesized that a heterozygous *Dcc* mutation might be sufficient to result in a neuroanatomical, neurophysiological, and motor phenotype, aiding in our understanding of the impairment of motor control seen in people carrying monoallelic *DCC* mutations.

Using axonal tract tracing, intra-cortical micro-stimulation, and behavioral tests, we found that pyramidal decussation was normal, as was corticospinal efficacy in producing responses in fore- and hindlimb muscles of adult *Dcc$^{+/-}$* mice, with no obvious functional impairments in their skilled motor control. Furthermore, no gait and posture dysfunctions were observed during treadmill locomotion, except for a decrease in the occurrence of out-of-phase walk and a longer duty cycle for the stance phase at slow treadmill speed. In spinal cord preparations isolated from neonatal mice, spinal interneuronal circuits exhibited normal locomotor pattern and rhythm; nevertheless, the flexor-related motoneuronal output was significantly increased in neonatal *Dcc$^{+/-}$* spinal cords. In summary, although *Dcc$^{+/-}$* mice do not exhibit any obvious bilateral impairments like those in humans, they exhibit subtle motor deficits during neonatal and adult locomotion.

MATERIALS AND METHODS

All animal procedures were performed in accordance with the [Author University] animal care committee's regulations. *Dcc*$^{+/-}$ mice were previously generated by the insertion of a neomycin resistance cassette into exon 3 of the *Dcc* gene (Fazeli et al., 1997). Immunoprecipitation experiments demonstrated that no full-length protein was produced from this allele in homozygous mutant mice (Fazeli et al., 1997).

DCC protein level quantification by western blotting

Spinal cords were dissected at E13.5, similarly to previously published (Langlois et al., 2010). Tissue was lysed with RIPA buffer (50 mM HEPES pH 7.4, 150 mM NaCl, 10% glycerol, 1.5 mM MgCl2, 1% Triton, 1% SDS, 1 mM EDTA) with protease inhibitors (Roche 11873580001) and boiled in SDS sample buffer for 5 min. Protein samples were separated by SDS-PAGE and then transferred to PVDF membrane. The membranes were incubated with 5% skim milk in TBST (0.01 M Tris-HCl pH 7.5, 150 mM NaCl, 0.1% Tween20) for one hour at room temperature, followed by primary antibody incubation (Goat anti-DCC,1:400, A-20, Santa Cruz Biotechnology and mouse anti-actin, 1:1000, SIGMA, cat# A5441) in 1% skim milk in TBST, overnight at 4°C. After 3 washes in TBST, membranes were incubated for 2 hours at room temperature, with secondary antibodies, which were conjugated to horseradish peroxidase (anti-goat HRP, 1:10000, Jackson ImmunoResearch, cat# 705-035-147 and anti-mouse-HRP, 1:10000, Jackson ImmunoResearch, cat# 115-035-003). After 3 washes in TBST and a final wash in TBS (without Tween20), western blots were visualized with chemiluminescence.

BDA tracing and analysis of the corticospinal tract

5 Adult WT and 5 *Dcc*$^{+/-}$ animals were anesthetized with ketamine/xylazine (100/10 mg/kg body weight) and a hand drill (Dremel) was used to create a small opening in the skull. 5µL of biotinylated dextran amine (10% in PBS, Molecular Probes, 10000 MW) was injected unilaterally into the motor cortex with a syringe (Hamilton, 80300) and the animal was sutured and allowed to recover. After 14 days, animals were perfused in 4% PFA in PBS and the spinal cord and brain were dissected and post-fixed in 4% PFA overnight before cryoprotection in 30% sucrose in PBS and freezing of segments in tissue freezing medium (O.C.T. compound). 30 µm cryosections of brain and spinal cord were incubated in streptavidin-488 (Jackson Immunoresearch, 1:200 in PBS + 0.1% Triton X-100) for 2 hours at room temperature, mounted, and imaged with a Leica DM4000 fluorescent microscope.

Intracortical microstimulation

Mice were anaesthetized with ketamine-xylazine (100/10 mg/kg body weight). When necessary, supplementary doses of ketamine were administered. The cranial bone was drilled to expose the motor cortex (approximate coordinates bregma +2 to -3, lateral 0.5 to 3). A tungsten electrode (0.1 MΩ) was inserted up to a depth of 0.7-0.8 mm. Cathodal pulses (10-80 µA, 0.2 ms duration, trains of 30 ms, interval 2.8 ms) were delivered through this electrode. A silver wire attached to the skin was used as the anode. To evoke motor response in the hindlimb, the electrode was positioned in the hindlimb representation of the motor cortex (about bregma -1 to -2 mm, lateral -1 to -2)

196 in 11 WT mice and 13 *Dcc*$^{+/-}$ mice. In 5 WT mice and 5 *Dcc*$^{+/-}$ mice, we stimulated the
197 forelimb caudal areas (bregma 0 to -1, lateral -1 to -2).

198 EMG probes organized in a duplex configuration (Ritter et al., 2014; Lemieux et
199 al., 2019) were inserted in the Tibialis Anterior (TA) on both sides. When we stimulated
200 the forelimb caudal area, we inserted EMG probes in the Biceps Brachialis (BB). For
201 technical reason, we did not attempt to record the ipsilateral BB. The threshold was
202 evaluated to evoke movements of the ankle and/or knee for the hindlimb and the wrist
203 and/or elbow for the forelimb. The threshold was defined as the current intensity
204 evoking movements 50% of the time or more. For EMG recordings, success rates,
205 latencies, and the number of motor spikes were quantified. We analyzed the number of
206 motor spikes rather than the amplitude of motor spikes because the number of spikes is
207 less dependent on the position of electrodes, which makes it a more reliable
208 approximation of the motor response.

209

210 *Skilled motor and locomotor behaviours*

211 *Cylinder test:* Unilateral and bilateral forelimb movements were assessed in a
212 glass beaker for the cylinder test, a vertical exploratory test (Bretzner et al., 2008;
213 Bretzner et al., 2010; Sparling et al., 2015). A mirror was placed behind the cylinder with
214 an angle in order to have an overall view of the mouse. Mice were videotaped for 20
215 rightings using a 40 Hz camera. The use of the left, right, or both forelimbs was scored
216 as the first paw contact (Figure 4A) and the total number of contacts (Figure 4B) for
217 each righting. To evaluate motor lateralization, the score was expressed as a

218 percentage of use of the left, right, or both forelimbs relative to the total number of first
219 or total forepaw contacts.

220 *Beam locomotion:* Motor coordination and balance were assessed while mice
221 crossed a wide (12 mm width) and a narrow (6 mm width) beam of 40 cm long each
222 (Luong et al., 2011; Fleming et al., 2013). After training, mice were videotaped at a
223 sampling frequency of 40Hz for three crossings. The number of steps, foot-slip errors,
224 and the time to cross the beam were quantified offline from videos. The percentage of
225 foot-slips was computed as the number of foot-slip errors relative of the number of steps
226 for each crossing and was then averaged for three trials per animal.

227 *Horizontal ladder locomotion:* Mice were trained to walk on a horizontal ladder with
228 a regular (1 cm spacing) rung arrangement pattern (Metz and Whishaw, 2002;
229 Laflamme et al., 2019). After training, mice were videotaped for three crossings using a
230 40 Hz camera. Videos were analyzed frame by frame to assess the number of steps,
231 foot-slip errors, and the time to cross the ladder. The percentage of foot-slip errors was
232 calculated as the number of errors relative of the number of steps for each trial. The
233 number of steps and the percentage of foot-slip errors were averaged for each mouse
234 for the three trials. The percentage of hindpaw slipping was not reported because it
235 happened only when mice fell from the ladder after forepaw slip.

236

237 *Treadmill locomotion*

238 8 WT and 9 *Dcc*$^{+/-}$ 6-month-old mice were placed on a treadmill (Cleversys
239 Systems Inc.) equipped with a transparent belt. The treadmill speed was adjusted at 15,
240 20, and 30 cm/s. Each mouse performed two 20 s trials at each speed (from lowest to

241 highest) and was allowed a three-minute rest between each trial. All mice were filmed
242 from below the belt with a high-frequency camera (100 frames/s, Basler) and videos
243 were analyzed offline using custom software as previously described (Lemieux et al.,
244 2016). To avoid acceleration and deceleration phases, videos were analyzed during
245 steady-state locomotion. The timing of lifts and contacts for all four limbs were extracted
246 manually and used for step cycle analysis by computing 1) stance duration: the interval
247 between the foot contact with the belt and the subsequent foot lift; 2) swing duration: the
248 interval between the foot lift and the next foot contact; 3) step cycle: the interval
249 between two successive foot contacts in each limb; and 4) stride frequency: the inverse
250 of the step cycle.
251
252 *Gait analysis during treadmill locomotion*
253 Locomotor gaits were defined by the interlimb coupling between stance phases of
254 four limbs and locomotor frequencies (number of step cycles per second). Using
255 custom-written routines in Matlab (The MathWorks), gaits of WT and *Dcc*$^{+/-}$ mice were
256 analyzed during treadmill locomotion at 15, 20, and 30 cm/s. As these speeds were low
257 to intermediate, analysis was focused on three gaits: out-of-phase walk, lateral walk,
258 and trot (Lemieux et al., 2016). Two slow walking gaits, pace and diagonal walk, were
259 excluded from the analysis due to their weak occurrence in mice.
260
261 *Neonatal locomotor-like activity*
262 Spinal cords from WT and *Dcc*$^{+/-}$ mice dissected out on postnatal day 1 to 3 were
263 used for *in vitro* experiments. Animals were anesthetized by intra-peritoneal injection of

ketamine/xylazine (100/10 mg/kg), decapitated, and eviscerated. Spinal cords were isolated by vertebrectomy at room temperature in oxygenated (95% O_2, 5% CO_2) artificial cerebrospinal fluid (aCSF) containing 127 mM NaCl, 3 mM KCl, 26 mM $NaHCO_3$, 1.25 mM NaH_2PO_4, 2 mM $CaCl_2$, 1mM $MgCl_2$, and 10 mM glucose. Spinal cords were cut at the thoracic Th10/11 and sacral S2/3 levels and placed ventral side up in a recording chamber superfused with oxygenated aCSF. Left and right lumbar L2 and L5 ventral roots were attached to suction electrodes designed and selected to fit the specific size of each recorded ventral root, thus ensuring a perfect seal of the suction electrode. The spinal cord was then allowed to recover for at least 30 minutes before electroneurographic (ENG) recording. Chemically evoked locomotor-like activity was induced by bath application of a cocktail of neurotransmitters: 5-hydrotryptamine (5-HT; 10 µM; Abcam) and an increased concentration of NMDA (2.5, 5, and 7.5 µM; Fisher) for episodes of about 30 minutes at each concentration. The signals were amplified (gain 2000) and band-pass filtered 10 Hz to 5 kHz (Qi-Ying Design). Signals were sampled at 50 KHz (Digidata 1440A, Axon Instruments) and stored on a PC (Axoscope 10.3; Molecular Device, California, USA) for offline analysis. The amplitude and duration of ENG bursts, the stride duration, the inter-burst duration, the duty cycle, and the coupling were analyzed on a 300 s epoch (25 to 60 locomotor cycles) of locomotor-like activity using Spinalcore. The amplitude was measured from the baseline (0) of integrated signals.

Statistics

Data for male and female mice were pooled together. Visual inspection suggested that the data were similar between sexes. Circular statistics was used to calculate the robustness of phase couplings between limbs or ENGs during locomotion; Rayleigh values are illustrated as the distance from the center of the polar plot (Drew and Doucet, 1991; Kjarrulff and Kiehn, 1996; Zar, 1996). A phase of 0 (or 1) indicates synchronization, whereas a phase of 0.5 corresponds to an alternation. The statistical significance of phase differences between WT and *Dcc*$^{+/-}$ mice was tested with a Watson-William test. Error bars shown are means ± standard deviations (SD) of the average or the coefficient of variation (CV). The normality of the distribution was assessed with Shapiro-Wilk prior to two-sample testing. Before pooling data, we tested the homogeneity of variances with a Fisher (two-samples, left and right limb) or Bartlett test (multiple samples, beam and horizontal ladder crossing). To detect differences between the mouse genotypes during adult treadmill locomotion, neonatal locomotor-like activity, and in anatomical measurements, we used the *t*-test or nonparametric Mann-Whitney ranked sum test when the variables did not fit a normal distribution (assessed by Kolmogorov-Smirnov test).

RESULTS

Skilled motor control and locomotion in Dcc$^{+/-}$ adult mice

In mice, rats, and cats, while locomotion on a smooth horizontal surface may rely solely on subcortical and spinal motor systems (Soblosky et al., 2001, Z'Graggen et al., 1998), the motor cortex plays an important role in the control of voluntary motor tasks such as skilled forelimb reaching (Whishaw 2000; Bretzner et al., 2008; Bretzner et al., 2010; Sparling et al., 2015), as well as skilled locomotion while the animal has to adjust its precise paw and limb trajectory to avoid obstacles (Drew et al., 1996; Metz and Whishaw 2002; Friel et al., 2007; Laflamme et al., 2019). Previous work showed that Dcc protein levels are reduced in the brain of adult *Dcc*$^{+/-}$ mice compared to WT mice (Flores et al., 2005). Using a test of vertical exploration to assess skilled motor control (Figure 1A-B), we quantified the percentage of initial and subsequent use of left, right, or both forepaws while reaching the wall of a cylinder during rearing. In comparison to control WT mice, the *Dcc*$^{+/-}$ mice displayed no differences in the percentage of use of their left, right, or both forepaws in the cylinder during the first contact on the wall (Figure 1A, n=6 WT and 7 *Dcc*$^{+/-}$ mice, Mann-Whitney test for left forepaw use, p=0.9226; right forepaw, p=0.6669; and both forepaws, p=0.5163), and during the total number of contacts (Figure 1B, Mann-Whitney test for total individual use of the left forepaw, p=0.2343; the right forepaw, p=0.5643; and both forepaws, p=0.3534), thus suggesting a normal use of forelimbs during vertical exploration.

To assess balance and motor coordination, we evaluated mice while they walked on a horizontal wide (12 mm width) or narrow (6 mm width) beam (Figure 1C-H). We

first assessed whether there was a learning effect on our measurements upon three beam crossings. As there were no significant effects on the number of steps, the time, and the percentage of foot-slips between the three crossings, data were pooled (Figure 1C-D and 1G-H, Bartlett or Fischer test, $p>0.05$, see Table 1-1 for statistics). Although both WT and *Dcc*$^{+/-}$ mice took more steps to cross the narrow beam than the wide one (Figure 1C, n= 6x3 WT and 7x3 *Dcc*$^{+/-}$ crossings, Mann-Whitney test, $p=0.0001$ for WT and $p=0.0011$ for *Dcc*$^{+/-}$ on the 6 versus 12 mm beam), no statistical differences were observed according to genotype (Figure 1C, Mann-Whitney test, $p=0.8392$ for WT versus *Dcc*$^{+/-}$ on the 6 mm beam; and $p=0.3193$ for WT versus *Dcc*$^{+/-}$ on the 12 mm beam). Similarly, the time to cross the wide beam was significantly shorter than to cross the narrow beam (Figure 1D, Mann-Whitney test, $p=0.0002$ for WT and $p=0.0011$ for *Dcc*$^{+/-}$ on the 6 versus 12 mm beam); nevertheless, no differences were found according to genotype (Figure 1D, Mann-Whitney test, $p=0.6145$ for WT versus *Dcc*$^{+/-}$ on the 6 mm beam; $p=0.8249$ for WT versus *Dcc*$^{+/-}$ on the 12 mm beam). The proportion of successful/failed crossings was not significantly different while crossing the wide or the narrow beam with the forelimbs (Figure 1E, Mann-Whitney test, $p=0.1398$ for the WT forelimbs and $p=0.1626$ for the *Dcc*$^{+/-}$ forelimbs on the 6 versus 12 mm beam) or the hindlimbs (Figure 1F, Mann-Whitney test $p=0.1534$ for the WT hindlimbs and $p=0.9456$ for the *Dcc*$^{+/-}$ hindlimbs on the 6 versus 12 mm beam). Among the failed crossings, the percentage of foot-slips was not significantly different with the forelimbs on the narrow beam (Figure 1G, n=7/18 WT and 12/21 *Dcc*$^{+/-}$ crossings, Mann-Whitney test, $p=0.8322$) or the hindlimbs on the narrow or wide beam (Figure 1H, n=10/18 WT and 7/21 *Dcc*$^{+/-}$ crossings on the narrow beam, Mann-Whitney test, $p=0.4336$; n=4/18 WT

and 6/21 *Dcc*$^{+/-}$ crossings on the wide beam, Mann-Whitney test, p=1) according to mouse genotype, thus supporting a proper locomotor balance and motor coordination in *Dcc*$^{+/-}$ mice.

To evaluate whether skilled forelimb locomotion might be impaired upon *Dcc* mutation, we also assessed mice while crossing a horizontal ladder with even-spaced rungs, a situation where there is a need for precise limb trajectories and paw placements. (Figure 1I-K). As with beam locomotion, we assessed whether there was a learning effect over the subsequent crossings. As there was no significant effect on the number of steps and the percentage of foot-slips over three crossings (Figure 1I and 1J, Bartlett test, p>0.05, see Table 1-1 for statistics), data were pooled. Both WT and *Dcc*$^{+/-}$ mice exhibited no statistical differences in the number of steps and in the percentage of foot-slips while walking on the rungs of the horizontal ladder (Figure 1I, Mann-Whitney test for the number of steps of n=18 WT vs. 21 *Dcc*$^{+/-}$ crossings, p=0.8840; Mann-Whitney test for the proportion of successful vs. failed crossings, p=0.6614). Among failed crossings, the percentage of foot-slips with the forelimb was also not significantly different according to genotype (Figure 1K, Mann-Whitney test, p=0.4091). Taken together, *Dcc*$^{+/-}$ mice display normal posture and balance overall, as well as normal skilled forelimb coordination and placement during skilled locomotion on a beam or a ladder.

Anatomy of the corticospinal tract in the adult mouse

A single-allele *Dcc* mutation is sufficient to alter pyramidal decussation and induce an aberrant bilateral misprojection of the corticospinal tract in humans (Srour et al.,

2010; Welniarz et al., 2017). Thus, we asked whether a heterozygous *Dcc* mutation in mice might also be sufficient to impair normal projection of the corticospinal tract. As shown in Figure 2, axonal tract tracing of the motor cortex revealed that the projection of corticospinal axons at the level of the pyramidal decussation (Figure 2B, middle panels) or post-decussation were similar in both $Dcc^{+/-}$ and WT mice (Figure 2B, right-most panels, 5 adult WT and 5 $Dcc^{+/-}$ animals), suggesting that the corticospinal tract projects normally in adult $Dcc^{+/-}$ mice. These results are consistent with previous observations (Welniarz et al., 2017).

Functional connectivity of the corticospinal tract in the adult mouse

While our anatomical studies revealed that corticospinal tract projection appears normal in $Dcc^{+/-}$ mice, the cortical representation and/or functional connectivity could still be impaired and evoke aberrant bilateral or ipsilateral movements in both fore- and hindlimb muscles. To test this hypothesis, we recorded motor and electromyographic (EMG) responses from bilateral fore- and hindlimb muscles evoked by intra-cortical micro-stimulation (ICMS) in the cortical caudal forelimb and hindlimb areas of adult WT and $Dcc^{+/-}$ adult mice. As shown in Figure 3A, ICMS applied within the cortical representation of the hindlimb evoked the strongest EMG responses in the contralateral hindlimb muscle, Tibialis Anterior (TA), and weaker responses in the ipsilateral TA muscle of WT and $Dcc^{+/-}$ mice at supra-threshold. To assess changes in corticospinal efficacy, we compared the threshold of cortically evoked motor responses in contralateral $Dcc^{+/-}$ and WT forelimb Biceps Brachialis (BB) and hindlimb TA muscles. Overall, there was no difference in the thresholds for evoking EMG responses in

394 contralateral WT and *Dcc*$^{+/-}$ fore- and hindlimb muscles (Figure 3B, Mann-Whitney test:
395 n=7 WT and 6 *Dcc*$^{+/-}$ for the TA, p=0.50; and n=5 WT and 5 *Dcc*$^{+/-}$ for the BB, p=0.34).
396 Moreover, the threshold for evoking contralateral motor responses in both fore- and
397 hindlimb was lower than that for evoking ipsilateral motor responses (Figure 3C,
398 Wilcoxon signed rank test: n=4 WT-Forelimbs, p=0.12; 2 *Dcc*$^{+/-}$-Forelimbs, p=0.5; 11
399 WT-Hindlimbs, p=9.7x10^{-4}; 13 *Dcc*$^{+/-}$-Hindlimbs p=4.9x10^{-4}), consistent with a proper
400 contralateral projection of the corticospinal tract. In pairs of muscles recorded with
401 EMGs, we found that the ipsilateral side was less excitable, sometimes not even
402 reaching the threshold criterion in contrast to the contralateral side in both WT and
403 *Dcc*$^{+/-}$ mice (Figure 3D, n=6 WT and 6 *Dcc*$^{+/-}$ mice). When there were sufficient
404 ipsilateral EMG responses around the threshold, we calculated latencies on both the
405 ipsi- and contralateral side (Figure 3E, Mann-Whitney test, n=4 pairs, p=0.74).
406 Latencies of ipsilateral EMG responses occurred systematically after contralateral ones,
407 but no differences were found between WT and *Dcc*$^{+/-}$ mice. The strength of the
408 response was evaluated as the number of motor spikes evoked upon intra-cortical
409 micro-stimulation. Although the number of motor spikes in contralateral muscles
410 appeared higher than in ipsilateral ones, it was not statistically different according to
411 genotype (Figure 3F, Wilcoxon signed rank test for contralateral vs. ipsilateral
412 responses: n=6 WT, p=0.22 and n=6 *Dcc*$^{+/-}$, p=0.31. Mann-Whitney test for WT vs.
413 *Dcc*$^{+/-}$: contralateral side, p=0.31; ipsilateral side, p=1). Furthermore, intra-cortical micro-
414 stimulation applied within the cortical representation of the hindlimb evoked specific
415 motor responses in hindlimb muscles—but never in forelimb muscles—in the mutant
416 mice (data not shown) and conversely the cortical representation of the forelimb never

evoked any responses in hindlimb muscles, thus demonstrating that corticospinal projections maintain their specificity. Together, these results show that the projection and functional connectivity of the corticospinal tract are preserved in adult *Dcc*$^{+/-}$ mice.

Treadmill locomotion in the adult mouse

Although *Dcc*$^{+/-}$ mice do not show impaired gross voluntary motor and locomotor behaviors, we hypothesized that the loss of one *Dcc* allele might cause more subtle changes in locomotor pattern and rhythm. To test that, we performed gait analysis of WT and *Dcc*$^{+/-}$ mice during treadmill locomotion at steady speeds of 15, 20, and 30 cm/s. Overall, the mean and coefficient of variation of the step cycle duration, the swing duration, the stance duration, and the duty cycle of the stance phase decreased as a function of treadmill speed for both WT and *Dcc*$^{+/-}$ mice (Figure 4). Although the duration of the step cycle and stance phase was normal, the duty cycle of the stance phase was significantly increased in *Dcc*$^{+/-}$ mice in comparison to their WT littermates at low and intermediate treadmill speeds (Figure 4D, n=8 WT and 10 *Dcc*$^{+/-}$ mice, duty cycle, Mann-Whitney test, p=0.0085 at 15 cm/s; unpaired student t-test, p=0.0490 at 20 cm/s, see Table 4-1 for statistics). Moreover, we also found a significant decrease in the variability of the duty cycle of the stance phase in *Dcc*$^{+/-}$ mice in comparison to WTs at 15 cm/s (Figure 4H, n=8 WT and 10 *Dcc*$^{+/-}$ mice, duty cycle, unpaired t test, p=0.0420 at 15 cm/s, see Table 4-1 for statistics). To look for changes in locomotor pattern as function of speed, we then plotted the duration of the stance and swing phase as function of step cycle duration. The linear regression did not show any significant differences according to genotype (Figure 5, n=8 WT and 10 Dcc+/- mice, F-test on

slopes, p=0.0503, F1, 497=3.85), thus suggesting overall a normal locomotor pattern in the *Dcc* heterozygous mice.

Given the bilateral locomotor disorganization in *Dcc* homozygous mutant spinal cords (Rabe Bernhardt et al., 2012), we also investigated the bilateral and homolateral coupling of limbs during treadmill locomotion. As shown by their polar plots (Figure 6A-C), the coupling between left-right forelimbs and hindlimbs, as well as the homolateral coupling between forelimbs and hindlimbs, were normal in $Dcc^{+/-}$ mice in comparison to their WT littermates (Watson-William test of WT versus $Dcc^{+/-}$: hindlimb coupling, p=0.71 at 15 cm/s, p=0.70 at 20 cm/s and p=0.99 at 30 cm/s; WT versus $Dcc^{+/-}$: forelimb coupling, p=0.77 at 15 cm/s, p=0.99 at 20 cm/s and p=0.71 at 30 cm/s; WT versus $Dcc^{+/-}$: homolateral coupling, p=0.98 at 15 cm/s, p=0.69 at 20 cm/s and p=0.95 at 30 cm/s). We also looked at phase coupling as function of locomotor frequency, which shows that the coordination between left and right forelimbs and hindlimbs was normal overall in $Dcc^{+/-}$ mice during locomotion at treadmill speeds from 15 to 30 cm/s (Figure 6D-F). Overall, these results show that locomotor pattern, rhythm, and interlimb coordination of $Dcc^{+/-}$ adult mice are normal.

As their WT littermates, $Dcc^{+/-}$ mice exhibited out-of-phase walk (i.e. asymmetrical walk), lateral walk, and trot with the predominance of trot at the highest treadmill speed tested of 30 cm/s (Figure 7). Interestingly, $Dcc^{+/-}$ mice exhibited significantly less out-of-phase walk than their WT littermates at the slowest treadmill speed of 15 cm/s (Figure 7B, n=8 WT and 10 $Dcc^{+/-}$, Mann Whitney test, p<0.0001 at 15 cm/s); nevertheless, its occurrence normalized at higher treadmill speeds of 20 and 30 cm/s (Figure 7B, no

462 significant differences between *Dcc*$^{+/-}$ and WT mice). Taken together, these analyses
463 suggest that the repertoire of gaits was overall normal in *Dcc*$^{+/-}$ mice.
464
465 ***Locomotor pattern and rhythm during neonatal locomotor-like activity***
466 Given that motor and locomotor controls appear to be normal in adult *Dcc*$^{+/-}$ mice,
467 we then assessed whether the loss of one WT allele of *Dcc* could impair the function of
468 isolated local spinal locomotor circuits. We first verified whether *Dcc*$^{+/-}$ developing spinal
469 cords have reduced Dcc protein levels. Western blots showed that Dcc protein levels
470 are reduced by ~50% in *Dcc*$^{+/-}$ embryonic spinal cords compared to WT spinal cords
471 (Figure 8, n= 6 embryos per genotype, Mann-Whitney test, p=0.002). This is consistent
472 with what has been observed previously in adult *Dcc*$^{+/-}$ mouse spinal cords (Liang et al.,
473 2014).
474 We next assessed whether the loss of one WT allele of *Dcc* could impair the
475 function of isolated local spinal locomotor circuits. To test this, we used spinal cords
476 isolated from neonatal WT and *Dcc*$^{+/-}$ mice, thus allowing us to study spinal circuits
477 without the influence of descending or peripheral input. As previously described (Kudo
478 and Yamada, 1987; Cazalets et al., 1992), locomotion was triggered by bath application
479 of a cocktail of 8 µM of 5HT and 2.5, 5, or 7.5 µM of NMDA to challenge spinal
480 interneuronal excitability. As illustrated by ENG bursts of L2 and L5 lumbar ventral root
481 activities (Figure 9A-B), locomotor-like activity was evoked at a low concentration of 2.5
482 µM of NMDA, but the activity was more regular and stable at an intermediate
483 concentration of 5 µM before decreasing in amplitude at a high concentration of 7.5 µM
484 in both WT and *Dcc*$^{+/-}$ mutant spinal cords (Figure 9F). Increasing the concentration of

NMDA statistically decreased the cycle duration, which translated into an increased duty cycle in both L2 and L5 ENG bursts for both WT and *Dcc*$^{+/-}$ spinal cords (Figure 9D). Nevertheless, no significant changes were found in cycle duration, burst duration, or duty cycle regarding the mouse genotype (see Table 9-1 for statistics), thus suggesting normal functioning of the spinal interneuronal circuit in *Dcc*$^{+/-}$ mice.

As shown in both WT and *Dcc*$^{+/-}$ spinal cord examples (Figure 9A-B), the ENG burst amplitude in L2 and L5 increased as a function of NMDA concentration from 2.5 µM to 5 µM and tended to decrease at a high concentration of 7.5 µM, below the amplitude level evoked at 2.5 µM. Interestingly, the amplitude of the L2 ENG burst of *Dcc*$^{+/-}$ spinal cords was significantly higher than that of WTs regardless of NMDA concentration (Figure 9F, n=4 WT and 7 *Dcc*$^{+/-}$, burst amplitude of WT vs. *Dcc*$^{+/-}$ L2 ENGs, Mann-Whitney test, p=0.0424 at 2.5 µM, p=0.0424 at 5 µM, p=0.0242 at 7.5 µM; see Table 9-1 for statistics). This increased motor output suggests that the spinal locomotor circuit (at least in the L2 segment) is more excitable upon bath application of NMDA in the developing spinal cord upon loss of one *Dcc* allele.

Variability in locomotor pattern and rhythm during neonatal locomotor-like activity

As previously shown in some mutant mouse studies (Zhang et al., 2008), *Dcc*$^{+/-}$ mutation might translate into a higher variability in locomotor pattern and rhythm during locomotion. To test this hypothesis, we quantified the coefficient of variation in locomotor features (Figure 10). Although ENG waveforms were more variable at low concentrations of NMDA (Figure 9A-B), overall, there were no significant differences in

the variability of cycle duration, burst duration, burst amplitude, and duty cycle (Figure 10A, n=4 WT and 7 *Dcc*$^{+/-}$, Mann-Whitney test for L2 cycle duration, p=0.0242, see Table 10-1 for statistics). Only the cycle duration of the L2 ENG waveform showed significantly higher variability in the *Dcc*$^{+/-}$ cycle duration of the L2 ENG in comparison to the WT.

Left-right and flexor-extensor coordination during neonatal locomotor-like activity

Although some mutant mice can produce a more variable locomotor coordination (Zhang et al., 2008), others produce a less variable one (Bellardita and Kiehn, 2015). As illustrated by polar plots (Figure 11, see Table 11-1 for statistics), the coordination between left-right flexor (Figure 11A), left-right extensor (Figure 11B) and flexor-extensor (Figure 11C) related ventral root activities were not significantly different according to the genotype (Watson-William test of WT versus *Dcc*$^{+/-}$: left-right L2 coupling, p=0.742 at 2.5 µM, p=0.890 at 5 µM and p=0.973 at 7.5 µM; WT versus *Dcc*$^{+/-}$: left-right L5 coupling, p=0.880 at 2.5 µM, p=0.954 at 5 µM and p=0.582 at 7.5 µM; WT versus *Dcc*$^{+/-}$: right L2-L5 coupling, p=0.705 at 2.5 µM, p=0.840 at 5 µM and p=0.894 at 7.5 µM). The variability of the coupling was not affected in *Dcc*$^{+/-}$ mice as evaluated with Mann-Whitney tests on Rayleigh values of WT versus *Dcc*$^{+/-}$ left-right L2 coupling: p=0.527 at 2.5 µM, p=0.527 at 5 µM, and 0.109 at 7.5 µM (Figure 11D); WT versus *Dcc*$^{+/-}$ left-right L5 coupling: p=0.629 at 2.5 µM, p=0.629 at 5 µM, and 0.857 at 7.5 µM (Figure 11E); WT versus *Dcc*$^{+/-}$ rL2-rL5 coupling, p=0.230 at 2.5 µM, p=0.412 at 5 µM, and 0.648 at 7.5 µM (Figure 11F). Overall, these results suggest a normal flexor-

extensor and left-right coordination regardless of the NMDA concentrations in *Dcc*$^{+/-}$ spinal cord preparations.

DISCUSSION

We show that adult mice lacking one allele of functional *Dcc* do not show impairments in skilled motor and locomotor control. In contrast to human individuals who have heterozygous *DCC* mutations, *Dcc* heterozygosity in mice does not promote an aberrant bilateral projection of the corticospinal tract or prevents its normal contralateral projection. The integrity of cortical representations and the functional connectivity of the corticospinal tract to forelimb and hindlimb motoneuronal pools are also preserved in *Dcc*$^{+/-}$ mice. On the other hand, although treadmill locomotion is mostly normal, the loss of one *Dcc* allele increases the duration and duty cycle of the stance phase, suggesting sensory feedback impairment. Moreover, although the spinal locomotor circuit appears functionally normal, *Dcc* heterozygous mutation increases the output of the flexor-related motoneuronal pool of isolated neonatal spinal cords. In summary, the heterozygous *Dcc* mouse does not replicate the motor phenotype of people affected with *DCC* haploinsufficiency, but it exhibits subtle motor differences that have not been reported so far.

Skilled motor control, motor cortex, and its corticospinal tract in adult *Dcc*$^{+/-}$ mice

Although the corticospinal tract and connectivity in the mouse are different from that of the human, previous studies using a spontaneous mutation allele that removes the exon encoding the P3 intracellular domain of DCC have shown that homozygous *Dcc*$^{kanga/kanga}$ and *Dcc*$^{kanga/-}$ mice exhibit a hopping gait, ataxia, and abnormal pyramidal

555 decussation through adulthood, thus recapitulating to some extent the motor phenotype
556 of *DCC* haploinsufficient individuals (Finger et al., 2002; Welniarz et al., 2017). We
557 therefore examined *Dcc* heterozygous mice and assessed the contribution of *Dcc* to
558 skilled motor and locomotor control, which relies on the integrity of the motor cortex and
559 its corticospinal tract (Pourchet et al., 2021). We found that $Dcc^{+/-}$ mice exhibited normal
560 asymmetrical control of the forelimb during vertical exploration in the cylinder test; they
561 also exhibited normal skilled forelimb coordination during voluntary locomotor control
562 while walking on a wide and narrow beam and while crossing a horizontal ladder.
563 Moreover, intracortical microstimulation applied within cortical representations of the
564 forelimb versus hindlimb evoked specific motor responses in forelimb or hindlimb
565 muscles, respectively, in the $Dcc^{+/-}$ mice, thus supporting the hypothesis that cortical
566 areas and their corticospinal projections maintain their specificity. The absence of
567 differences in cortical representations and the absence of differences in synaptic
568 connectivity or latency of the corticospinal tract axons to the spinal cord in $Dcc^{+/-}$ mice
569 argue that cortical representation and functional connectivity of the corticospinal tract
570 are normal in $Dcc^{+/-}$ mice.

571

572 **Increased duration of the duty cycle of the stance phase of adult $Dcc^{+/-}$**
573 **mice during treadmill locomotion**

574 In contrast to the hopping gait of $Dcc^{kanga/kanga}$ and $Dcc^{kanga/-}$ mutant mice (Finger
575 et al., 2002; Welniarz et al., 2017) or conditional ablation of *Dcc* in *HoxB8*-expressing
576 spinal neurons (Peng et al., 2018), we found no defects in locomotor gait of adult $Dcc^{+/-}$

mice during treadmill locomotion. Although we only assessed *Dcc*$^{+/-}$ mice at slow and intermediate walking speeds, no events of hop or gallop were observed during brief locomotor accelerations when the animals sped up to reach a locomotor frequency of 5-6 Hz. Among our locomotor data, the duty cycle of the stance phase was significantly increased in *Dcc*$^{+/-}$ mice, especially at slow walking speed. Given the absence of changes in the duration of flexor and extensor-related locomotor activities and in their coupling during locomotor-like activity even at high NMDA concentrations using isolated spinal cord preparations, the increased duration of the duty cycle of the stance phase of *Dcc*$^{+/-}$ mice might reflect a sensory feedback deficit. In support to this idea, Netrin-1/Dcc signaling guides sensory axons (Lakhina et al., 2012; Laumonnerie et al., 2014): *Netrin-1* and *Dcc*$^{-/-}$ spinal cords exhibit an aberrant projection of cutaneous and proprioceptive axons in the spinal cord (Watanabe et al., 2006; Masuda et al., 2008; Laumonnerie et al., 2014) and *Dcc* is required for the normal development of nociceptive processing in mice and humans (da Silva et al., 2018). Furthermore, removing sensory afferents of semi-intact spinal cord preparations shortens the duration of the extensor phase during locomotion (Juvin et al., 2007); therefore, an aberrant sensory feedback in *Dcc*$^{-/-}$ mice could presumably increase the duty cycle of their stance phase. Further studies will be necessary to test this hypothesis in mice and humans with the heterozygous mutation.

Spinal locomotor circuits are normal but show increased motoneuronal output modulation in neonatal *Dcc*$^{+/-}$ mice

598 Using spinal cords isolated from neonatal mice, we also investigated the spinal
599 locomotor circuit in the absence of descending input from the brain and sensory
600 feedback from the periphery. In contrast to *Dcc*$^{-/-}$ or *Dcc*$^{kanga/kanga}$ spinal cords (Rabe
601 Bernhardt et al., 2012), those with *Dcc*$^{+/-}$ mutation had normal coordination between left
602 and right and between flexor- and extensor-related motoneuronal output modulation
603 during neonatal locomotion. Moreover, there were no significant differences in
604 locomotor pattern and rhythm regardless of NMDA concentrations. However, the
605 amplitude of the flexor-related motoneuronal activity was significantly increased in *Dcc*$^{+/-}$
606 spinal cords upon bath application of NMDA, suggesting that DCC plays a role in the
607 establishment of the neuronal circuit modulating the excitability of the spinal locomotor
608 circuit. Nevertheless, this increased output in flexor-related motoneuronal activity did not
609 persist through adulthood, suggesting that sensory feedback might readjust the
610 motoneuronal output of adult mutant mice. Perhaps comparative electromyographic
611 studies of stepping in newborn, adolescent, and adult humans carrying monoallelic *DCC*
612 mutations would reveal similar abnormalities during bipedal walking or quadrupedal
613 crawling (Patrick et al., 2009; Vasudevan et al., 2016).

614

615 **Conclusion**

616 In summary, our study finds that, in contrast to humans, a heterozygous mutation
617 in *Dcc* has little effect on skilled and basic locomotor control, or on the normal
618 functioning of the motor cortex and its corticospinal connectivity. Although no functional
619 impairments were found either in locomotor pattern and rhythm of spinal cord

preparations isolated from neonatal mice, the flexor-related motoneuronal output was significantly increased in the developing spinal cord of *Dcc*$^{+/-}$ mice. However, this increase in flexor-related motoneural output did not persist through adulthood and locomotor gait was overall normal, albeit with a longer duty cycle and less out-of-phase walk. This finding raises the possibility of the existence of subtle locomotor changes in humans carrying monoallelic *DCC* mutations.

References

Bellardita, C., and Kiehn, O. (2015). Phenotypic characterization of speed-associated gait changes in mice reveals modular organization of locomotor networks. Curr. Biol. 25, 1426-1436.

Braisted, J.E., Catalano, S.M., Stimac, R., Kennedy, T.E., Tessier-Lavigne, M., Shatz, C.J., and O'Leary, D.D. (2000). Netrin-1 promotes thalamic axon growth and is required for proper development of the thalamocortical projection. J. Neurosci. 20, 5792-5801.

Bretzner, F., Liu, J., Currie, E., Roskams, A.J., and Tetzlaff, W. (2008). Undesired effects of a combinatorial treatment for spinal cord injury--transplantation of olfactory ensheathing cells and BDNF infusion to the red nucleus. Eur. J. Neurosci. 28, 1795-1807.

Bretzner, F., Plemel, J.R., Liu, J., Richter, M., Roskams, A.J., and Tetzlaff, W. (2010). Combination of olfactory ensheathing cells with local versus systemic cAMP treatment after a cervical rubrospinal tract injury. J. Neurosci. Res. 88, 2833-2846.

Cazalets, J.R., Sqalli-Houssaini, Y., and Clarac, F. (1992). Activation of the central pattern generators for locomotion by serotonin and excitatory amino acids in neonatal rat. J. Physiol. 455, 187-204.

da Silva, R.V., Johannssen, H.C., Wyss, M.T., Roome, R.B., Bourojeni, F.B., Stifani, N., Marsh, A.P.L., Ryan, M.M., Lockhart, P.J., Leventer, R.J., *et al.* (2018). DCC Is

646 Required for the Development of Nociceptive Topognosis in Mice and Humans. Cell.
647 Rep. 22, 1105-1114.

648 Ding, Y.Q., Kim, J.Y., Xu, Y.S., Rao, Y., and Chen, Z.F. (2005). Ventral migration of
649 early-born neurons requires Dcc and is essential for the projections of primary afferents
650 in the spinal cord. Development 132, 2047-2056.

651 Dominici, C., Moreno-Bravo, J.A., Puiggros, S.R., Rappeneau, Q., Rama, N., Vieugue,
652 P., Bernet, A., Mehlen, P., and Chedotal, A. (2017). Floor-plate-derived netrin-1 is
653 dispensable for commissural axon guidance. Nature 545, 350-354.

654 Drew, T., and Doucet, S. (1991). Application of circular statistics to the study of
655 neuronal discharge during locomotion. J. Neurosci. Methods 38, 171-181.

656 Drew, T., Jiang, W., Kably, B., and Lavoie, S. (1996). Role of the motor cortex in the
657 control of visually triggered gait modifications. Can. J. Physiol. Pharmacol. 74, 426-442.

658 Fazeli, A., Dickinson, S.L., Hermiston, M.L., Tighe, R.V., Steen, R.G., Small, C.G.,
659 Stoeckli, E.T., Keino-Masu, K., Masu, M., Rayburn, H.*, et al.* (1997). Phenotype of mice
660 lacking functional Deleted in colorectal cancer (Dcc) gene. Nature 386, 796-804.

661 Finger, J.H., Bronson, R.T., Harris, B., Johnson, K., Przyborski, S.A., and Ackerman,
662 S.L. (2002). The netrin 1 receptors Unc5h3 and Dcc are necessary at multiple choice
663 points for the guidance of corticospinal tract axons. J. Neurosci. 22, 10346-10356.

664 Fleming, S.M., Ekhator, O.R., and Ghisays, V. (2013). Assessment of sensorimotor
665 function in mouse models of Parkinson's disease. J. Vis. Exp. (76). doi, 10.3791/50303.

666 Flores, C., Manitt, C., Rodaros, D., Thompson, K.M., Rajabi, H., Luk, K.C., Tritsch, N.X.,
667 Sadikot, A.F., Stewart, J., and Kennedy, T.E. (2005). Netrin receptor deficient mice
668 exhibit functional reorganization of dopaminergic systems and do not sensitize to
669 amphetamine. Mol. Psychiatry 10, 606-612.

670 Friel, K.M., Drew, T., and Martin, J.H. (2007). Differential activity-dependent
671 development of corticospinal control of movement and final limb position during visually
672 guided locomotion. J. Neurophysiol. 97, 3396-3406.

673 Izzi, L., and Charron, F. (2011). Midline axon guidance and human genetic disorders.
674 Clin. Genet. 80, 226-234.

675 Jain, R.A., Bell, H., Lim, A., Chien, C.B., and Granato, M. (2014). Mirror movement-like
676 defects in startle behavior of zebrafish dcc mutants are caused by aberrant midline
677 guidance of identified descending hindbrain neurons. J. Neurosci. 34, 2898-2909.

678 Jiang, Z., Carlin, K.P., and Brownstone, R.M. (1999). An in vitro functionally mature
679 mouse spinal cord preparation for the study of spinal motor networks. Brain Res. 816,
680 493-499.

681 Juvin, L., Simmers, J., and Morin, D. (2007). Locomotor rhythmogenesis in the isolated
682 rat spinal cord: a phase-coupled set of symmetrical flexion extension oscillators. J.
683 Physiol. 583, 115-128.

684 Keino-Masu, K., Masu, M., Hinck, L., Leonardo, E.D., Chan, S.S., Culotti, J.G., and
685 Tessier-Lavigne, M. (1996). Deleted in Colorectal Cancer (DCC) encodes a netrin
686 receptor. Cell 87, 175-185.

687 Kjaerulff, O., and Kiehn, O. (1996). Distribution of networks generating and coordinating
688 locomotor activity in the neonatal rat spinal cord in vitro: a lesion study. J. Neurosci. 16,
689 5777-5794.

690 Kudo, N., and Yamada, T. (1987). N-methyl-D,L-aspartate-induced locomotor activity in
691 a spinal cord-hindlimb muscles preparation of the newborn rat studied in vitro. Neurosci.
692 Lett. 75, 43-48.

693 Kullander, K., Butt, S.J., Lebret, J.M., Lundfald, L., Restrepo, C.E., Rydstrom, A., Klein,
694 R., and Kiehn, O. (2003). Role of EphA4 and EphrinB3 in local neuronal circuits that
695 control walking. Science 299, 1889-1892.

696 Laflamme, O.D., Lemieux, M., Thiry, L., and Bretzner, F. (2019). DSCAM Mutation
697 Impairs Motor Cortex Network Dynamic and Voluntary Motor Functions. Cereb. Cortex
698 29, 2313-2330.

699 Lakhina, V., Marcaccio, C.L., Shao, X., Lush, M.E., Jain, R.A., Fujimoto, E., Bonkowsky,
700 J.L., Granato, M., and Raper, J.A. (2012). Netrin/DCC signaling guides olfactory
701 sensory axons to their correct location in the olfactory bulb. J. Neurosci. 32, 4440-4456.

Langlois, S.D., Morin, S., Yam, P.T., and Charron, F. (2010). Dissection and culture of commissural neurons from embryonic spinal cord. J. Vis. Exp. (39). pii: 1773. doi, 10.3791/1773.

Laumonnerie, C., Da Silva, R.V., Kania, A., and Wilson, S.I. (2014). Netrin 1 and Dcc signalling are required for confinement of central axons within the central nervous system. Development 141, 594-603.

Lemieux, M., and Bretzner, F. (2019). Glutamatergic neurons of the gigantocellular reticular nucleus shape locomotor pattern and rhythm in the freely behaving mouse. PLoS Biol. 17, e2003880.

Lemieux, M., Josset, N., Roussel, M., Couraud, S., and Bretzner, F. (2016). Speed-Dependent Modulation of the Locomotor Behavior in Adult Mice Reveals Attractor and Transitional Gaits. Front. Neurosci. 10, 42.

Liang, D.Y., Zheng, M., Sun, Y., Sahbaie, P., Low, S.A., Peltz, G., Scherrer, G., Flores, C., and Clark, J.D. (2014). The Netrin-1 receptor DCC is a regulator of maladaptive responses to chronic morphine administration. BMC Genomics 15, 345-2164-15-345.

Luong, T.N., Carlisle, H.J., Southwell, A., and Patterson, P.H. (2011). Assessment of motor balance and coordination in mice using the balance beam. J. Vis. Exp. (49). pii: 2376. doi, 10.3791/2376.

720 Masuda, T., Watanabe, K., Sakuma, C., Ikenaka, K., Ono, K., and Yaginuma, H. (2008).
721 Netrin-1 acts as a repulsive guidance cue for sensory axonal projections toward the
722 spinal cord. J. Neurosci. 28, 10380-10385.

723 Meneret, A., Franz, E.A., Trouillard, O., Oliver, T.C., Zagar, Y., Robertson, S.P.,
724 Welniarz, Q., Gardner, R.J.M., Gallea, C., Srour, M.*, et al.* (2017). Mutations in the
725 netrin-1 gene cause congenital mirror movements. J. Clin. Invest. 127, 3923-3936.

726 Metz, G.A., and Whishaw, I.Q. (2002). Cortical and subcortical lesions impair skilled
727 walking in the ladder rung walking test: a new task to evaluate fore- and hindlimb
728 stepping, placing, and co-ordination. J. Neurosci. Methods 115, 169-179.

729 Patrick, S.K., Noah, J.A., and Yang, J.F. (2009). Interlimb coordination in human
730 crawling reveals similarities in development and neural control with quadrupeds. J.
731 Neurophysiol. 101, 603-613.

732 Peng, J., and Charron, F. (2013). Lateralization of motor control in the human nervous
733 system: genetics of mirror movements. Curr. Opin. Neurobiol. 23, 109-118.

734 Peng, J., Ferent, J., Li, Q., Liu, M., Da Silva, R.V., Zeilhofer, H.U., Kania, A., Zhang, Y.,
735 and Charron, F. (2018). Loss of Dcc in the spinal cord is sufficient to cause a deficit in
736 lateralized motor control and the switch to a hopping gait. Dev. Dyn. 247, 620-629.

737 Pourchet, O., Morel, M.P., Welniarz, Q., Sarrazin, N., Marti, F., Heck, N., Gallea, C.,
738 Doulazmi, M., Roig Puiggros, S., Moreno-Bravo, J.A.*, et al.* (2021). Loss of floor plate

739 Netrin-1 impairs midline crossing of corticospinal axons and leads to mirror movements.
740 Cell. Rep. 34, 108654.

741 Powell, A.W., Sassa, T., Wu, Y., Tessier-Lavigne, M., and Polleux, F. (2008).
742 Topography of thalamic projections requires attractive and repulsive functions of Netrin-
743 1 in the ventral telencephalon. PLoS Biol. 6, e116.

744 Rabe Bernhardt, N., Memic, F., Gezelius, H., Thiebes, A.L., Vallstedt, A., and Kullander,
745 K. (2012). DCC mediated axon guidance of spinal interneurons is essential for normal
746 locomotor central pattern generator function. Dev. Biol. 366, 279-289.

747 Rabe, N., Gezelius, H., Vallstedt, A., Memic, F., and Kullander, K. (2009). Netrin-1-
748 dependent spinal interneuron subtypes are required for the formation of left-right
749 alternating locomotor circuitry. J. Neurosci. 29, 15642-15649.

750 Ritter, L.K., Tresch, M.C., Heckman, C.J., Manuel, M., and Tysseling, V.M. (2014).
751 Characterization of motor units in behaving adult mice shows a wide primary range. J.
752 Neurophysiol. 112, 543-551.

753 Schott, G.D., and Wyke, M.A. (1981). Congenital mirror movements. J. Neurol.
754 Neurosurg. Psychiatry. 44, 586-599.

755 Serradj, N., Paixao, S., Sobocki, T., Feinberg, M., Klein, R., Kullander, K., and Martin,
756 J.H. (2014). EphA4-mediated ipsilateral corticospinal tract misprojections are necessary
757 for bilateral voluntary movements but not bilateral stereotypic locomotion. J. Neurosci.
758 34, 5211-5221.

759 Soblosky, J.S., Song, J.H., and Dinh, D.H. (2001). Graded unilateral cervical spinal cord
760 injury in the rat: evaluation of forelimb recovery and histological effects. Behav. Brain
761 Res. 119, 1-13.

762 Sparling, J.S., Bretzner, F., Biernaskie, J., Assinck, P., Jiang, Y., Arisato, H., Plunet,
763 W.T., Borisoff, J., Liu, J., Miller, F.D., and Tetzlaff, W. (2015). Schwann cells generated
764 from neonatal skin-derived precursors or neonatal peripheral nerve improve functional
765 recovery after acute transplantation into the partially injured cervical spinal cord of the
766 rat. J. Neurosci. 35, 6714-6730.

767 Srivatsa, S., Parthasarathy, S., Britanova, O., Bormuth, I., Donahoo, A.L., Ackerman,
768 S.L., Richards, L.J., and Tarabykin, V. (2014). Unc5C and DCC act downstream of
769 Ctip2 and Satb2 and contribute to corpus callosum formation. Nat. Commun. 5, 3708.

770 Srour, M., Riviere, J.B., Pham, J.M., Dube, M.P., Girard, S., Morin, S., Dion, P.A.,
771 Asselin, G., Rochefort, D., Hince, P.*, et al.* (2010). Mutations in DCC cause congenital
772 mirror movements. Science 328, 592.

773 Talpalar, A.E., Bouvier, J., Borgius, L., Fortin, G., Pierani, A., and Kiehn, O. (2013).
774 Dual-mode operation of neuronal networks involved in left-right alternation. Nature 500,
775 85-88.

776 Thiry, L., Lemieux, M., D Laflamme, O., and Bretzner, F. (2016). Role of DSCAM in the
777 development of the spinal locomotor and sensorimotor circuits. J. Neurophysiol. 115,
778 1338-1354.

779 Varadarajan, S.G., Kong, J.H., Phan, K.D., Kao, T.J., Panaitof, S.C., Cardin, J.,
780 Eltzschig, H., Kania, A., Novitch, B.G., and Butler, S.J. (2017). Netrin1 Produced by
781 Neural Progenitors, Not Floor Plate Cells, Is Required for Axon Guidance in the Spinal
782 Cord. Neuron 94, 790-799.e3.

783 Vasudevan, E.V., Patrick, S.K., and Yang, J.F. (2016). Gait Transitions in Human
784 Infants: Coping with Extremes of Treadmill Speed. PLoS One 11, e0148124.

785 Watanabe, K., Tamamaki, N., Furuta, T., Ackerman, S.L., Ikenaka, K., and Ono, K.
786 (2006). Dorsally derived netrin 1 provides an inhibitory cue and elaborates the 'waiting
787 period' for primary sensory axons in the developing spinal cord. Development 133,
788 1379-1387.

789 Welniarz, Q., Morel, M.P., Pourchet, O., Gallea, C., Lamy, J.C., Cincotta, M., Doulazmi,
790 M., Belle, M., Meneret, A., Trouillard, O.*, et al.* (2017). Non cell-autonomous role of
791 DCC in the guidance of the corticospinal tract at the midline. Sci. Rep. 7, 410-017-
792 00514-z.

793 Zar, J.H. (1996). Biostatistical Analysis: 3rd Edition. Prentice Hall Inc., Upper Saddle
794 River Edition.

795 Z'Graggen, W.J., Metz, G.A., Kartje, G.L., Thallmair, M., and Schwab, M.E. (1998).
796 Functional recovery and enhanced corticofugal plasticity after unilateral pyramidal tract
797 lesion and blockade of myelin-associated neurite growth inhibitors in adult rats. J.
798 Neurosci. 18, 4744-4757.

799 Zhang, Y., Narayan, S., Geiman, E., Lanuza, G.M., Velasquez, T., Shanks, B., Akay, T.,
800 Dyck, J., Pearson, K., Gosgnach, S., Fan, C.M., and Goulding, M. (2008). V3 spinal
801 neurons establish a robust and balanced locomotor rhythm during walking. Neuron 60,
802 84-96.

803 **Figure legends**

804

805 **Figure 1: Skilled motor control in adult *Dcc*$^{+/-}$ and WT mice.** (A-B) Percentage of first
806 and total contacts on the wall while rearing in the cylinder test. (C-H) Mean number of
807 steps (C), time (D), percentage of successful and failed trials with the forelimb (E) and
808 hindlimb (F), percentage of foot slips with the forelimb (G) and hindlimb (H) among trials
809 with errors. (I-K) Mean number of steps (I), percentage of successful and failed trials (J),
810 and percentage of foot slips among failed trials (K) during locomotion on the rungs of a
811 horizontal ladder. WT in black and *Dcc*$^{+/-}$ in gray. * indicates $p<0.05$, ** indicates $p<0.01$,
812 and *** indicates $p<0.001$, (see Table 1-1 for statistics).

813

814 **Figure 2: Projections of the corticospinal tract in *Dcc*$^{+/-}$ and WT mice.** (A)
815 Schematic drawing of transverse brainstem sections showing a unilateral corticospinal
816 tract axon bundle (grey area) as it projects from the left motor cortex to the contralateral
817 dorsal funiculus. (B) BDA tracing of the corticospinal tract of 3-month-old WT and *Dcc*$^{+/-}$
818 mice shows no difference in the projection of corticospinal tract axons at the level of the
819 pyramidal decussation.

820

821 **Figure 3: *Dcc*$^{+/-}$ adult mice exhibit normal lateralization of the corticospinal tract.**
822 (A) Examples of EMG activity of contralateral and ipsilateral Tibialis Anterior (TA). A
823 30ms train of cathodal pulses (duration 0.2 ms, interval 2.8 ms) was delivered in either

the caudal forelimb area or the hindlimb area. Bottom, higher temporal resolution of the contralateral trace illustrates latency and response (motor spikes raster) measurements. (B) Left, threshold for evoking activity in the contralateral Biceps Brachialis (BB). Right, threshold for evoking activity in the contralateral TA. Threshold is defined as motor spikes elicited in at least 50% of trials. (C) Thresholds for pairs of hindlimbs (HL, circle) or forelimbs (FL, square). Contralateral is on the x-axis and ipsilateral on the y-axis. (D) Success rate (percentage) for evoking an EMG response vs. the threshold of the contralateral side. Dashed line indicates the threshold, defined as a success rate of 50%. Data are for pairs of muscle recorded with EMGs. Contralateral is in black and ipsilateral in gray. (E) Left, ipsilateral vs. contralateral averaged latencies for pairs of muscles recorded with EMGs. Middle, an example of EMG traces to illustrate the delay between contralateral and ipsilateral sides. Right, boxplot of contralateral to ipsilateral delays. (F) Averaged number of motor spikes evoked by ICMS for the contralateral (x-axis) and ipsilateral (y-axis) sides. WT in black and *Dcc*$^{+/-}$ in gray.

Figure 4: Locomotor pattern of adult *Dcc*$^{+/-}$ and WT mice during treadmill locomotion. (A-D) Mean and (E-H) coefficient of variation of step cycle duration (A and E), swing duration (B and F), stance duration (C and G), and duty cycle of the stance phase (D and H) of WT and *Dcc*$^{+/-}$ mice at 3 different treadmill speeds (15, 20, and 30 cm/s). WT in black and *Dcc*$^{+/-}$ in gray. * indicates $p<0.05$ and ** indicates $p<0.01$, (see Table 4-1 for statistics).

Figure 5: Swing and stance duration as functions of step cycle duration during treadmill locomotion. Swing (top panels (A and B) and stance (bottom panels (C and D) duration as functions of step cycle duration of WT and *Dcc*$^{+/-}$ mice. Note 3 different treadmill speeds were combined. WT in black and *Dcc*$^{+/-}$ in grey.

Figure 6: Bilateral and homolateral interlimb coordination during treadmill locomotion. (A-C), Polar plots showing the mean vector for the relationships between left and right forelimbs (A), left and right hindlimbs (C), and between homolateral fore- and hindlimb (B) of WT (black circles) and *Dcc*$^{+/-}$ (gray circles) at treadmill speeds of 15, 20, and 30 cm/s. The position on the polar plot indicates mean phase; the distance from the center of the polar plot indicates strength of the coupling (Rayleigh). Symbols represent individual mice at a treadmill speed of 20 cm/s, vectors represent the mean phase coupling of WT and *Dcc*$^{+/-}$ groups at 15, 20, and 30 cm/s. Dashed inner circles represent a Rayleigh value of 0.5. (D-F) Phase of the coupling between left and right forelimbs (D), hindlimbs (F), and (E) forelimb-hindlimb as a function of locomotor frequency during treadmill locomotion at 15-30 cm/s. WT in black and *Dcc*$^{+/-}$ in gray.

Figure 7: Locomotor gait occurrence during treadmill locomotion. (A) Gray-scaled matrixes of the percentage of occurrence of a gait (column) at 15, 20, and 30 cm/s (row) for WT and *Dcc*$^{+/-}$ mice. The sum of a row equals 100%. (B) Box plots representing the percentage of gait occurrence at 15, 20, and 30 cm/s. **** indicates $p<0.0001$.

867

868 **Figure 8: Dcc protein levels in *Dcc*$^{+/-}$ and WT spinal cords.** Left, Western blot of Dcc
869 in embryonic WT and *Dcc*$^{+/-}$ spinal cords. *Dcc control* is a cell lysate over-expressing a
870 *Dcc* cDNA. Right, Dcc/actin ratio relative to WT (*Dcc*$^{+/+}$). ** indicates p<0.01.

871

872 **Figure 9: Locomotor pattern and rhythm during neonatal locomotor-like activity.**
873 (A-B) Examples of L5 and L2 ENG recordings of WT (A) and *Dcc*$^{+/-}$ (B) mice upon bath
874 application of drugs (8 µM of 5HT and 2.5, 5, or 7.5 µM of NMDA). (C-J) Mean and data
875 of cycle duration (C and G), burst duration (D and H), duty cycle (E and I), and burst
876 amplitude (F and J) of WT and *Dcc*$^{+/-}$ L2 (C-F) and L5 (G-J) ENGs at different NMDA
877 concentrations (8 µM of 5HT and 2.5, 5, or 7.5 µM of NMDA). * indicates p<0.05, (see
878 Table 9-1 for statistics).

879

880 **Figure 10: Variability in electroneurographic (ENG) waveforms during neonatal**
881 **locomotor-like activity.** Mean and coefficients of variation of cycle duration (A and E),
882 burst duration (B and F), duty cycle (C and G), and burst amplitude (D and H) of WT
883 (black circles) and *Dcc*$^{+/-}$ (grey triangles) of L2 (A-D) and L5 (E-H) ENG waveforms at
884 different NMDA concentrations. * indicates p<0.05, (see Table 10-1 for statistics).

885

886 **Figure 11: Locomotor coupling during neonatal locomotor-like activity. (A-C)**
887 Polar plots showing the mean vector (arrows) for the relationships between left and right
888 L2 (A, lL2 vs. rL2) and L5 (B, lL5 vs. rL5), and between homolateral flexor and extensor

(C, rL2 vs. rL5) of WT (top polar plots) and *Dcc*$^{+/-}$ (bottom polar plots) spinal cord preparations at low (2.5 µM, lighter grey arrow), intermediate (5 µM, darker grey arrow), and high (7.5 µM, black arrow) NMDA concentrations. The position on the polar plot indicates mean phase; the distance from the center of the polar plot indicates strength of the coupling (Rayleigh). For clarity, individual data are shown only for the highest concentration (black symbols for WT and grey symbols for Dcc$^{+/-}$). Dashed inner circles represent a Rayleigh value of 0.5. (D-F) Boxplots of the Rayleigh score at three NMDA concentrations between left and right L2 (D), left and right L5 (E), and between homolateral L2-L5 (F). Abbreviations: rL2=right L2 ventral root; lL2=left L2 ventral root; rL5=right L5 ventral root; lL5=left L5 ventral root (see Table 11-1 for statistics).

Extended Data table 1-1: Skilled motor control in adult *Dcc*$^{+/-}$ and WT mice.

Extended Data table 4-1: Locomotor pattern of adult *Dcc*$^{+/-}$ and WT mice during treadmill locomotion.

Extended Data table 9-1: Locomotor pattern and rhythm during neonatal locomotor-like activity.

Extended Data table 10-1: Variability in electroneurographic (ENG) waveforms during neonatal locomotor-like activity.

Extended Data table 11-1: Locomotor coupling during neonatal locomotor-like activity.

Cylinder test

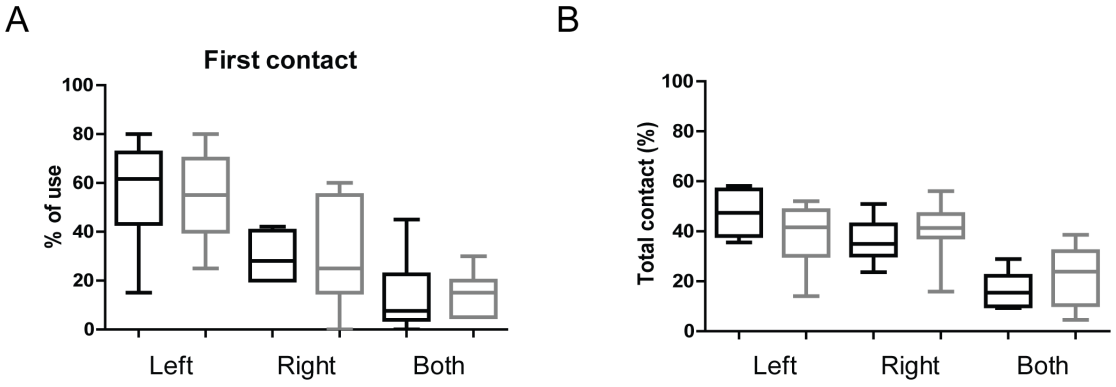

Beam locomotion

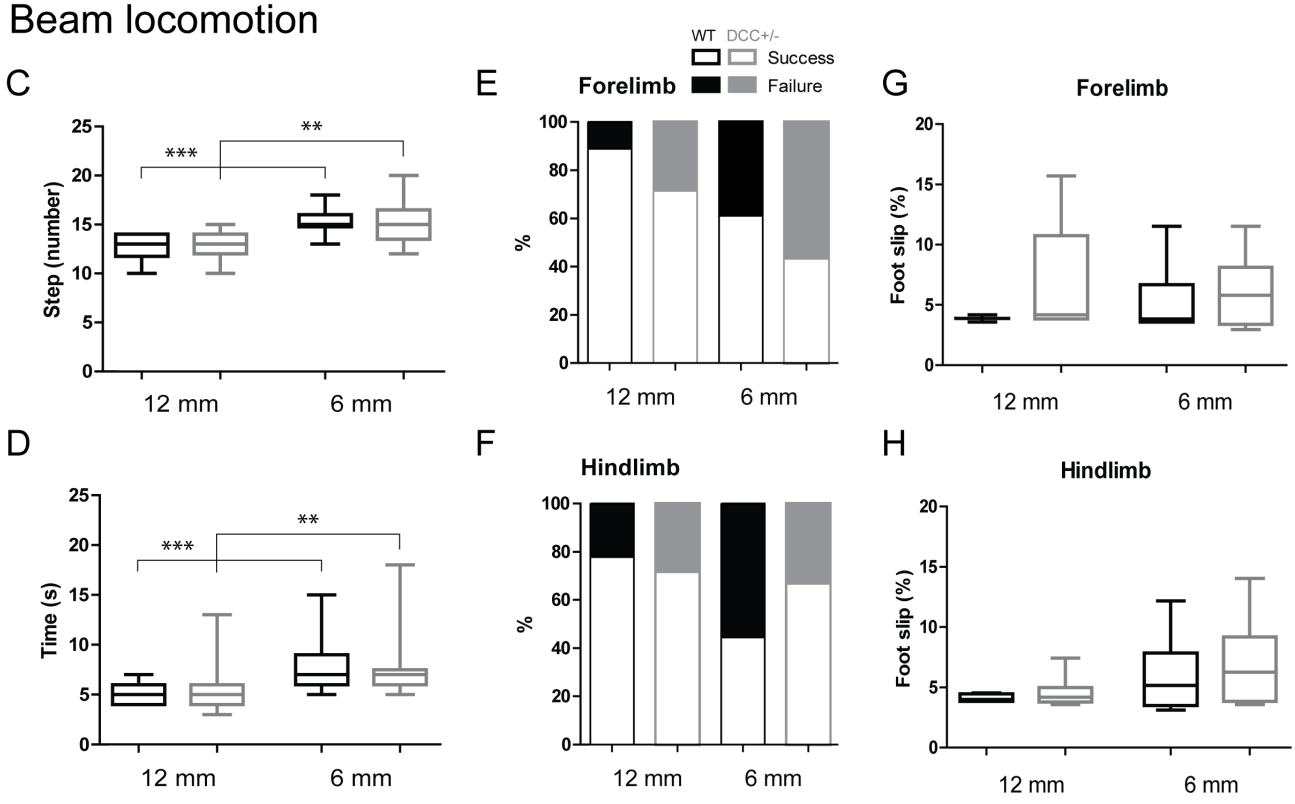

Ladder locomotion

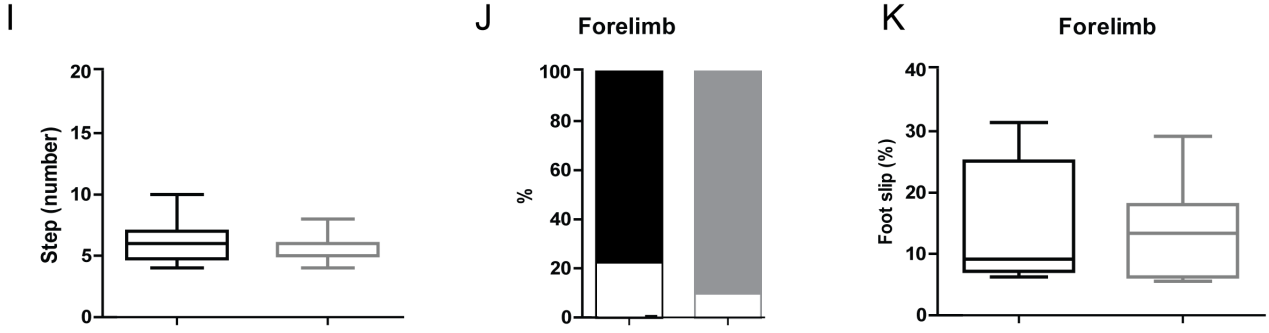

A

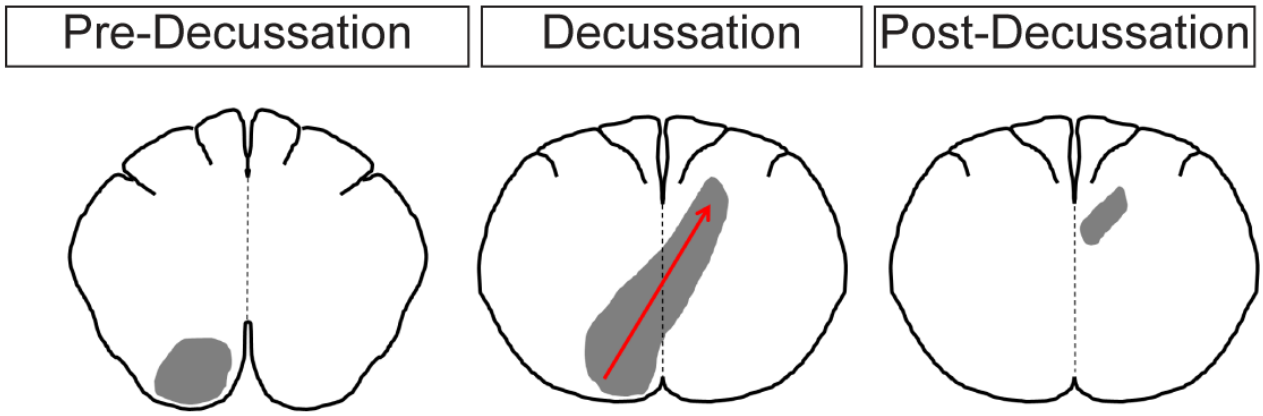

B